

# Impacts of the Differential Phase of Incident Waves on the Polarimetric Variables from Hail

Valery Melnikov, *Member, IEEE*, Dusan Zrnić *Life Fellow, IEEE*, and Djordje Mirković

**Abstract**— It is shown that in the simultaneous dual polarization radar mode, the differential phase ( $\beta$ ) between the orthogonally polarized waves impinging on hail affects the polarimetric variables. This effect is caused by interference of the polarized waves scattered by non-spherical particles. The  $\beta$ -impact is considered for dry hail and water-coated hailstones. For the hailstones' canting angles oriented uniformly relative to the vertical, reflectivity and differential reflectivity do not depend on  $\beta$ , but the correlation coefficient between the polarized waves and phase upon scattering do. Tumbling of falling hailstones is considered using the Fisher distribution of the orientation angles. It is shown that the  $\beta$ -impact enhances with increasing tumbling. The  $\beta$ -impact should be considered in hail detection methods utilizing the correlation coefficient. The potential of using the differential phase upon scattering in hail detection and sizing is also discussed.

**Index Terms**—Polarimetric weather radar, polarimetric variables, scattering from hail, hail signature.

## I. INTRODUCTION

Detection of hail in thunderstorms is one of the main missions of weather radars. To forecast and detect hail, the US National Weather Service has been using its S band weather radar network (WSR-88D also known as NEXRAD) for decades. Before 2013, hail was detected using radar reflectivity, its height profile, and thermodynamic cloud parameters [1, 2]. A recent study of relations between radar reflectivity ( $Z$ ) and the giant hail size does not show a correlation [3] that could be because of the scattering resonance effects. It was found that the wind fields play a major role in hailstorms producing giant hail [3]. In 2013, the radars were upgraded to dual polarization, and methods to detect hail using  $Z$ , differential reflectivity ( $Z_{DR}$ ) [4-7], and correlation coefficient between received electromagnetic waves at orthogonal polarizations ( $\rho_{hv}$ ) [8-10] have been developed. A fuzzy-logic combination of these three variables is currently in use in hail detection and sizing with WSR-88Ds [11]. The theoretical foundations used to interpret data in the above-cited articles are based on spheroidal models having smooth surfaces. Advances in electromagnetic modeling [12-13] allow considerations of natural [14-16] or artificial [17] hailstone shapes. Recent advances and the current state of radar hail detection and sizing are summarized in [16].

Most dual polarization weather radars utilize simultaneous transmission of orthogonally polarized waves frequently called SHV mode (Simultaneously transmitted and received

Horizontally and Vertically polarized waves). The differential phase ( $\beta$ ) of the impinging waves is caused by propagation through clouds and/or precipitation and by radar hardware. The latter phase shift is called the differential phase upon transmission ( $\psi_t$ ) and is caused by differences in the signal paths in radar hardware creating horizontally and vertically polarized transmitted waves. Scattering of waves by non-spherical particles leads to interference of the primary and depolarized scattered waves and can bias  $Z_{DR}$  [18]. The phase  $\beta$  affects the interference intensity. These effects were analyzed in [19] for ice cloud particles. To our knowledge, these impacts have not been considered for hail and that is the focus of our study.

## II. BASIC RELATIONS

### A. Radar Polarimetric Variables

The radar polarimetric variables from hydrometeors are calculated using the scattering matrix  $S$ . Let  $E_{hi}$  and  $E_{vi}$  be the amplitudes of horizontally (subscript h) and vertically (subscript v) polarized waves impinging (subscript i) on a scatterer. Then, the received voltages  $e_{hr}$  and  $e_{vr}$  from a single scatterer can be written as,

$$\begin{pmatrix} e_{hr} \\ e_{vr} \end{pmatrix} = \begin{pmatrix} C_{Rh} & 0 \\ 0 & C_{Rv} \end{pmatrix} \begin{pmatrix} 1 & 0 \\ 0 & e^{j\gamma} \end{pmatrix} \begin{pmatrix} S_{hh} & S_{hv} \\ S_{hv} & S_{vv} \end{pmatrix} \begin{pmatrix} 1 & 0 \\ 0 & e^{j\beta} \end{pmatrix} \begin{pmatrix} E_{hi} \\ E_{vi} \end{pmatrix}, \quad (1)$$

where  $C_{Rh}$  and  $C_{Rv}$  are the radar constants (the range dependence is included) for the horizontal and vertical polarization channels [18],  $\beta = \varphi_{dp} + \psi_t$  is the impinging phase with  $\varphi_{dp}$  being the one-way propagation differential phase and  $\psi_t$  is the differential phase upon transmission (DPT),  $\gamma = \varphi_{dp} + \psi_r$  with  $\psi_r$  being the receiver differential phase. Phases  $\psi_r$  and  $\psi_t$  may differ because the signal paths in a radar transmitter and a receiver are different. Eq. (1) does not account for differential attenuation, but that has no bearing on the  $\beta$ -effects.

The measured differential phase  $\Phi_{DP}$  is

$$\Phi_{DP} = 2\varphi_{dp} + \psi_t + \psi_r + \delta = \beta + \gamma + \delta, \quad (2)$$

where  $\delta$  is the differential phase upon scattering. The constants  $C_{Rh,v}$  in (1) are obtained from radar calibration and are important in the  $Z$  and  $Z_{DR}$  measurements; all other radar variables are independent of these constants. We consider a calibrated radar and known  $C_{Rh,v}$ , hence  $E_{hi}$  and  $E_{vi}$  can be considered equal, therefore, they and  $C_{Rh,v}$  can be omitted in further discussion of the  $\beta$ -effects. Then (1) simplifies to

Funding was provided by NOAA/Office of Oceanic and Atmospheric Research under NOAA-University of Oklahoma Cooperative Agreement #NA21OAR4320204, U.S. Department of Commerce. This article contains supplemental materials with figures labeled with S, for instance, Fig. S1.

V. Melnikov is affiliated with Cooperative Institute for Severe and High-Impact Weather Research and Operations (CIWRO), the University of Oklahoma, and NOAA/OAR National Severe Storms Laboratory, Norman, OK 73072 (e-mail: [Valery.Melnikov@noaa.gov](mailto:Valery.Melnikov@noaa.gov)).

D. S. Zrnić is affiliated with NOAA/OAR National Severe Storms Laboratory, and School of Meteorology, and School of Electrical and Computer Engineering, University of Oklahoma, Norman, OK 73072 (e-mail: [Dusan.Zrnic@noaa.gov](mailto:Dusan.Zrnic@noaa.gov)).

D. Mirkovic is affiliated with Cooperative Institute for Severe and High-Impact Weather Research and Operations (CIWRO), the University of Oklahoma, and NOAA/OAR National Severe Storms Laboratory, Norman, OK 73072 (e-mail: [Djordje.Mirkovic@noaa.gov](mailto:Djordje.Mirkovic@noaa.gov)).

> REPLACE THIS LINE WITH YOUR MANUSCRIPT ID NUMBER (DOUBLE-CLICK HERE TO EDIT) <

$$e_{hr} = S_{hh} + S_{hv}e^{j\beta} \text{ and } e_{vr} = (S_{vv}e^{j\beta} + S_{hv})e^{j\gamma}. \quad (3)$$

Radar receives the scattered waves from all particles in the resolution volume and resulting voltage is

$$E_{hr} = \sum_n e_{hr}^{(n)} \exp(ikr_n), \quad (4)$$

where  $n$  numerates the scatterers and  $\exp(ikr_n)$  accounts for the range  $r_n$  from radar to the  $n^{\text{th}}$  scatterer. The time-dependent exponent is omitted in (4) without loss of substance. An equation similar to (4) can be written for  $E_{vr}$  by replacing the subscript  $h$  with  $v$ .

The received power in the channel with the horizontally polarized wave is

$$P_h = \langle E_{hr}^* E_{hr} \rangle, \quad (5)$$

where the brackets stand for ensemble averaging and the asterisk indicates complex conjugate. The averaging is performed over the sizes, shapes, orientations, and distances  $r_n$ . Assuming that the scattering amplitudes do not depend on  $r_n$ , the averaging over  $r_n$  can be separated from other averaging. Then range reshuffling of the scatterers leads to

$$P_h = \langle N(D) e_{hr}^*(\theta, \varphi, \alpha, D) e_{hr}(\theta, \varphi, \alpha, D) \rangle, \quad (6)$$

where  $N(D)$  is the size distribution of the scatterers with  $D$  being a characteristic size of the scatterer (e.g., its maximum dimension) and the sum in (4) is replaced with the mean product and the brackets stand for averaging over the sizes, shapes, and orientation angles  $\theta, \varphi$ , and  $\alpha$  defined in Fig. 1.

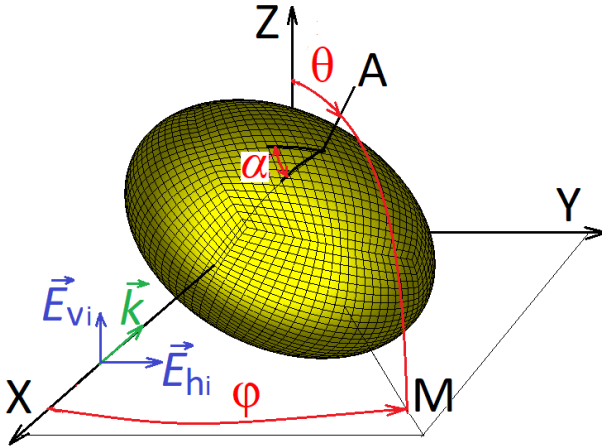


Fig. 1. Scattering geometry for an oriented spheroid.

To study the  $\beta$ -effects, we consider scattering by spheroids because a) the current WSR-88D's hail detection algorithm is based on this model and b) this model allows for understanding of the main features of the effect.

The frame XYZ of scattering geometry (Fig. 1) is placed at the scatterers' center and its XY plane is horizontal. The spheroid's minor axis  $A$  makes the angle  $\theta$  (the canting angle) with the vertical. A projection of the spheroid's minor axis to the XY plane defines the point  $M$  and the angle  $\varphi$  between the X axis and projection. Angle  $\alpha$  is an angle of rotation of the spheroid around its minor axis. Angles  $\theta, \varphi$ , and  $\alpha$  are the Euler angles. It is assumed that  $E_{vi}$  is directed along the Z axis, i.e., the radar antenna elevation angle is zero. The direction of

propagation of the impinging wave (the vector  $\mathbf{k}$  in the figure) coincides with the X axis.

Assuming independence of the scatterers' orientation angles from their sizes and shapes, averaging over orientations can be performed for a scatterer having a given size and shape. This may not hold in nature because our knowledge of hailstones' dynamics is limited. Then, for a given size  $D$ :

$$P_h(D) = N(D) \langle e_{hr}^*(\theta, \varphi, \alpha, D) e_{hr}(\theta, \varphi, \alpha, D) \rangle_{\theta, \varphi, \alpha}, \quad (7)$$

where the subscripts at the brackets denote averaging over the angles. Then, using (3)  $P_h(D)$  and  $P_v(D)$  can be written as,

$$\langle P_h(D) \rangle = N(D) [\langle |S_{hh}|^2 \rangle_{\theta, \varphi, \alpha} + 2\text{Re}(\langle S_{hh}^* S_{hv} \rangle_{\theta, \varphi, \alpha} e^{j\beta}) + \langle |S_{hv}|^2 \rangle_{\theta, \varphi, \alpha}], \quad (8)$$

and

$$\langle P_v(D) \rangle = N(D) [\langle |S_{vv}|^2 \rangle_{\theta, \varphi, \alpha} + 2\text{Re}(\langle S_{vv}^* S_{hv} \rangle_{\theta, \varphi, \alpha} e^{-j\beta}) + \langle |S_{hv}|^2 \rangle_{\theta, \varphi, \alpha}], \quad (9)$$

where  $\text{Re}(x)$  stands for the real part of  $x$ .

Differential reflectivity  $Z_{DR}$ , correlation coefficient  $\rho_{hv}$ , and phase upon scattering  $\delta$  are obtained as,

$$Z_{DR}(D) = 10 \log(\langle P_h \rangle / \langle P_v \rangle) \quad (\text{dB}), \quad (10)$$

$$\rho_{hv}(D, \beta) = N(D) | \langle e_{hr}^*(\theta, \varphi, \alpha, D) e_{vr}(\theta, \varphi, \alpha, D) \rangle | / (\langle P_h \rangle \langle P_v \rangle)^{1/2}, \quad (11)$$

and

$$\delta(D, \beta) = \arg(\langle e_{hr}^*(\theta, \varphi, \alpha, D) e_{vr}(\theta, \varphi, \alpha, D) \rangle) 180/\pi - \beta - \gamma \quad (\text{deg}), \quad (12)$$

where the subscripts  $\theta, \varphi, \alpha$  are omitted to shorten notations. The phase  $\delta$  enters in the measured  $\Phi_{DP}$  (2), so, to obtain  $\delta$  from (2), phase  $\beta + \gamma$  must be subtracted from the argument of correlation function. It follows from (3) that the vertically polarized wave acquires the phase  $\gamma$  relative to the phase of the horizontally polarized wave. Because  $\delta$  is obtained from the argument of  $\langle e_{hs}^* e_{vs} \rangle$ , the phase  $\gamma$  in  $e_{vr}$  does not affect  $\delta$  and for computational purposes we can set  $\gamma = 0$ , then

$$\delta(D, \beta) = \arg(\langle e_{hs}^*(\theta, \varphi, \alpha, D) e_{vs}(\theta, \varphi, \alpha, D) \rangle) 180/\pi - \beta \quad (\text{deg}). \quad (13)$$

If backscattering does not change the phase between the scattered polarized waves (for instance, if a scatterer is a sphere), then  $\delta = 0$  regardless of  $\beta$ . The correlation function in (13) is written as,

$$\langle e_{hs}^*(\theta, \varphi, \alpha, D) e_{vs}(\theta, \varphi, \alpha, D) \rangle = \langle S_{hh}^* S_{vv} \rangle e^{j\beta} + \langle S_{hh}^* S_{hv} \rangle + \langle S_{hv}^* S_{vv} \rangle + \langle |S_{hv}|^2 \rangle e^{-j\beta}. \quad (14)$$

The values of  $Z_{DR}(D)$ ,  $\rho_{hv}(D, \beta)$ , and  $\delta(D, \beta)$  for hailstones of various sizes  $D$  are presented in section III. It is also shown in section III that  $P_h$ ,  $P_v$ , and  $Z_{DR}$  are independent of  $\beta$  at the uniform distribution of  $\varphi$ , and therefore, we do not indicate  $\beta$  in their arguments in (7)-(10). For spheroids, the scattering properties do not depend on  $\alpha$ , and, therefore, it is omitted in the further discussion. For natural nonsymmetric hailstones, averaging over  $\alpha$  is needed.

### B. Angular averaging

Hailstones tumble in the air, and the orientation angles  $\theta$  and  $\varphi$  change over time. To perform averaging over these angles, a probability distribution  $W(\theta, \varphi)$  should be defined. We assume

> REPLACE THIS LINE WITH YOUR MANUSCRIPT ID NUMBER (DOUBLE-CLICK HERE TO EDIT) <

a uniform distribution in angle  $\varphi$  ( $0 \leq \varphi < 360^\circ$ ) in the horizontal plane OXY (Fig. 1). The Gaussian distribution of canting angle determined in the polarization plane has been used (e.g., [6]), which is an approximation that breaks at wide distributions. The Fisher distribution correctly describes  $W(\theta, \varphi)$  for all possible  $\theta$  and  $\varphi$  ([20] chapter 8, [21] section 2.3.6).

Free falling hailstones change their orientations in time. Terms “tumbling” and “tumbling intensity” are used here for this change in  $\theta$  and its dispersion. This change is characterized by the mean canting angle  $\langle \theta \rangle$  determined as the mean deviations of the spheroid’s minor axis from the vertical orientation. For the Fisher distribution, the standard deviation in canting angles ( $\sigma_\theta$ ) depends on  $\langle \theta \rangle$ . Weak tumbling has small  $\langle \theta \rangle$ , and  $\langle \theta \rangle$  increases with increasing tumbling. At random tumbling,  $\langle \theta \rangle = 90^\circ$ . Little is known about hailstones tumbling and we show our results for moderate ( $\langle \theta \rangle = 20^\circ$ ), strong ( $\langle \theta \rangle = 40^\circ$ ), and random ( $\langle \theta \rangle = 90^\circ$ ) tumbling.

For the uniform distribution in  $\varphi$ ,  $W(\theta, \varphi)$  depends on  $\theta$  only, i.e.,

$$W(\theta, \varphi) = \frac{\mu}{4\pi \sinh(\mu)} \exp(\mu \cos \theta), \quad \mu \geq 0, \quad (15)$$

$$\int_0^{2\pi} d\varphi \int_0^\pi \sin \theta W(\theta, \varphi) d\theta = 1.$$

The parameter  $\mu$  is related to  $\langle \theta \rangle$  and  $\sigma_\theta$  via:

$$\langle \theta \rangle = \int_0^{2\pi} d\varphi \int_0^\pi \theta \sin \theta W(\theta, \varphi) d\theta,$$

$$\sigma_\theta^2 = \int_0^{2\pi} d\varphi \int_0^\pi (\theta^2 - \langle \theta \rangle^2) \sin \theta W(\theta, \varphi) d\theta. \quad (16)$$

Relations between  $\langle \theta \rangle$ ,  $\sigma_\theta$ , and  $\mu$  are depicted in the Supplemental material (Fig. S1). The relation between  $\langle \theta \rangle$  and  $\sigma_\theta$  is almost linear up to  $\langle \theta \rangle = 50^\circ$  (the right panel in Fig. S1). We indicate  $\langle \theta \rangle$  and the corresponding  $\sigma_\theta$  in the computational results in section III.

The product  $\langle S_{hh}^* S_{hv} \rangle$  in (8), (9), and (14) can be written using  $W(\theta, \varphi)$  as,

$$\langle S_{hh}^* S_{hv} \rangle = \int_0^{2\pi} d\varphi \int_0^\pi S_{hh}^*(\theta, \varphi) S_{hv}(\theta, \varphi) \sin \theta W(\theta, \varphi) d\theta. \quad (17)$$

Other moments are written similarly. The product of matrix elements in (17) depends on the size and shape of a scatterer as well as on  $\langle \theta \rangle$ . The matrix coefficients for a scatterer of any shape can be obtained using software for solving electromagnetic problems. We have used the WIPL-D package [12, 22].

### III. COMPUTATIONAL RESULTS

Hailstones have a variety of shapes: some are close to spheroids with smooth surfaces; large hailstones (sizes  $> 4$  cm) frequently have rough surfaces [14-17] affecting their scattering properties. To study the impacts of  $\beta$  on the polarimetric variables, we have modeled hailstones with spheroids of various sizes and oblateness. We also consider hailstones covered with a water film frequently called “wet” hailstones.

Oblate spheroids are characterized with a maximal size  $D$  and a ratio of minor ( $b$ ) to major ( $a$ ) semiaxes ( $b/a < 1$ ). For spheroids,  $D = 2a$  and  $b/a$  is a measure of oblateness. The most frequent hailstones’  $b/a$  lay in the interval 0.6 – 0.8 [23, 24]. In this section, we present our results for  $b/a = 0.7$  and results for

$b/a = 0.6$  and 0.8 are in the Supplemental materials. Our results show that the  $\beta$ -dependencies of  $\delta$  and  $\rho_{hv}$  exhibit periodicity of  $180^\circ$ . Therefore, the  $\beta$ -dependencies are shown in the interval  $0 - 180^\circ$ . For completely random tumbling,  $Z_{DR} = 0$  dB hence  $Z_{DR}$  panels are not shown.

Our results are presented here for selected sizes to analyze the main features of  $\beta$ -dependencies. The size distributions of hailstones are quite variable (e.g., [16]). To assess the  $\beta$ -impact on collections of hailstones, one should assume a distribution of  $\langle \theta \rangle$  for hailstones of various sizes, which is unknown. Non-spherical shapes of hailstones most likely result from non-chaotic tumbling, especially for large hailstones. Not completely random tumbling could result in various water content on their surfaces. The assessment of the  $\beta$ -impacts on collection of hailstones of different sizes will require a thorough analysis of the assumptions to be made.

#### A. Dry hailstones

To study the  $\beta$ -impacts on the radar variables from hail, we have used hail density of  $0.92 \text{ g cm}^{-3}$ . Our results show that  $\beta$  does not affect  $Z$  and  $Z_{DR}$  if the canting angle  $\theta$  is distributed symmetrically relative to the vertical (top panels in Fig. 2). This is because  $\langle S_{hh}^* S_{hv} \rangle_{\theta, \varphi} = 0$  in this case.

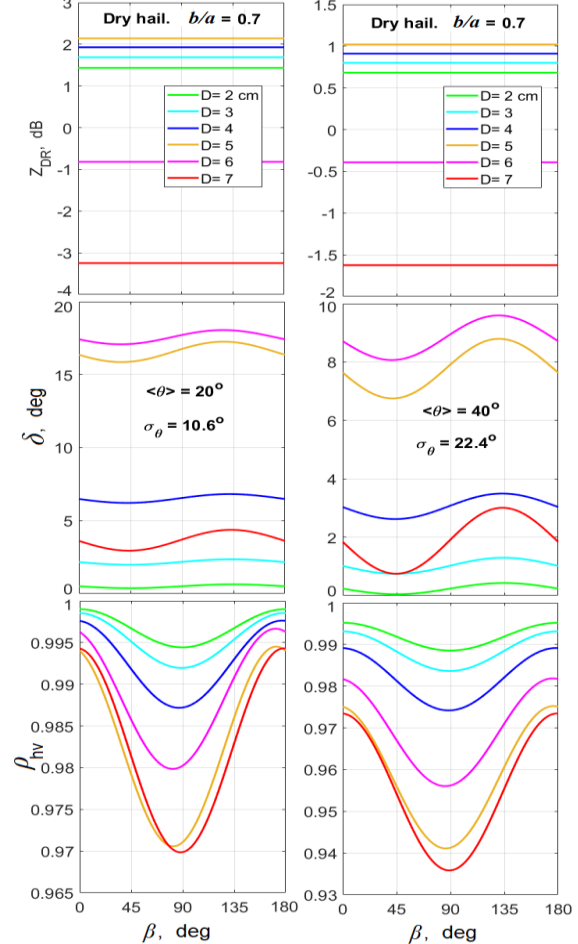


Fig. 2. Dry hailstones. (Left column):  $Z_{DR}$ ,  $\delta$ , and  $\rho_{hv}$  as functions of  $\beta$  for  $\langle \theta \rangle = 20^\circ$ ,  $b/a = 0.7$ . S band. (Right column): as in the left column but for  $\langle \theta \rangle = 40^\circ$ .



> REPLACE THIS LINE WITH YOUR MANUSCRIPT ID NUMBER (DOUBLE-CLICK HERE TO EDIT) <

Significantly severe hailstones ( $D > 5$  cm, the size name adopted from [25]) can produce negative  $Z_{DR}$  discussed in [9,14] (see also the top panels in Fig. 2). One can see that the  $Z_{DR}$  values remain negative up to strong tumbling that makes such values informative for the detection of significantly severe hail. Negative  $Z_{DR}$  at the top of Z cores can be produced by conical graupel [28].

In [23], the  $\delta$  values larger than  $5^\circ$  are attributed to wet hail. Our results show that dry hail of  $D > 3$  cm can produce  $\delta > 5^\circ$  (the central panels in Figs. 2, S2, S5, and S6). The  $\delta$  typically increases with size up to  $D = 5$  cm (Figs. 2, S2, S3, S5, and S6) and exhibits weak dependencies on  $\beta$ . For significantly severe hail ( $D > 5$  cm), the resonance effects can bring  $\delta$  to the values characteristic of smaller sizes. One can also see that  $\delta$  increases with decreasing  $b/a$  and  $\delta$  decreases at stronger tumbling which introduces an uncertainty in the relation between  $\delta$  and size. To estimate the hail size, all dual polarization variables should be considered.

At completely random tumbling,  $\delta$  does not become zero at any  $\beta$  as  $Z_{DR}$  does (left panels in Figs. 3, S4, and S7) because despite symmetry in the orientation angles  $\theta$  and  $\varphi$ , this geometry is not completely symmetrical for the impinging orthogonally polarized waves shifted in phase [19]. One can also see that  $\delta(\beta)$  can change the sign. The amplitude of the  $\delta$  variations is small for dry hail at  $\langle \theta \rangle = 90^\circ$ , but significantly increases for wet hail (subsection B).

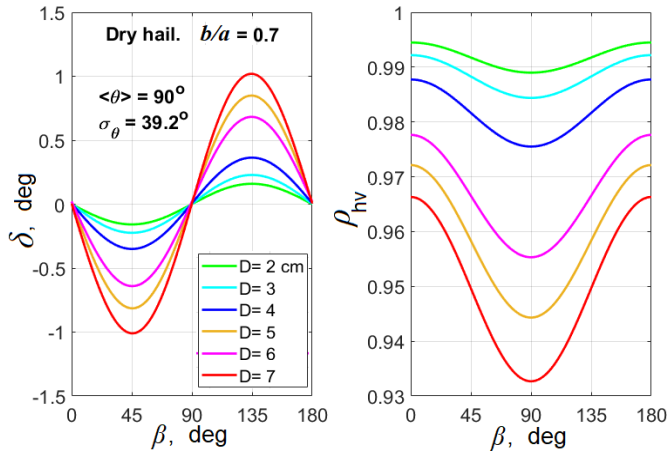


Fig. 3. As in Fig. 2 but for random tumbling

The authors of [23, Table 2] indicate that the bulk values of  $\rho_{hv}$  from hail at S band are larger than 0.95. But in [23], the authors consider polarimetric variables that are not obtained in the SHV mode whereas we explore the effects of that mode. Our results show that significantly severe dry hail can produce  $\rho_{hv} < 0.95$  (right bottom panel in Figs. 3, the right panels in S6, and S7). Non-spheroidal hailstones can also produce these values [14]. The values of  $\rho_{hv}$  strongly depend on  $\beta$ . For instance, at  $D = 4$  cm  $\rho_{hv}$  drops from 0.990 at  $\beta = 0^\circ$  to 0.975 at  $\beta = 90^\circ$  and  $\langle \theta \rangle = 40^\circ$  (Fig. 2, right column). Generally,  $\rho_{hv}$  decreases with the hail size, but the  $\beta$ -impact introduce uncertainty to this dependence. The  $\beta$ -impact increases for more oblate hailstones (right panels in Figs. S5-S7).  $\rho_{hv}$  attains its minimum at  $\beta = 90^\circ$  regardless of the hail size and tumbling

intensity. It is problematic to quantitatively use  $\rho_{hv}$  from hail without knowing  $\beta$ .

### B. Wet hailstones

Hailstones can be covered with liquid water films during wet growth [26, 27] and due to melting and/or collision with raindrops below the melting layer. Such hailstones are frequently called ‘wet’. In our calculations, the maximal thickness of the water cover has been obtained from [26], where the mass of water cover  $M_w$  retained on the hailstone’s surface is defined as,  $M_w = 0.268 + 0.139 M_i$  (g), and  $M_i$  is mass of the ice core in g. The thickness of the water film is depicted in Fig. S8.

$Z_{DR}(D)$  for horizontally oriented dry and wet hailstones with  $b/a = 0.7$  are quite different (Fig. 4, left). Dry hailstones produce negative  $Z_{DR}$  at  $D > 6$  cm, whereas wet ones exhibit negative  $Z_{DR}$  at  $D > 4$  cm and  $Z_{DR}(D)$  is more complicated because of a stronger resonance effect. Generally, negative  $Z_{DR}$  indicates hail regardless of wetness. Conical graupel can also produce negative  $Z_{DR}$  [28]. Graupel typically produces higher  $\rho_{hv}$  than large hail and that can be used to distinguish between these types of hydrometeors [23]. Tumbling reduces absolute  $Z_{DR}$  values, but these can remain negative at resonance sizes even at moderate and strong  $\langle \theta \rangle$  (Figs. 5, S11, S12, S14, and S15).

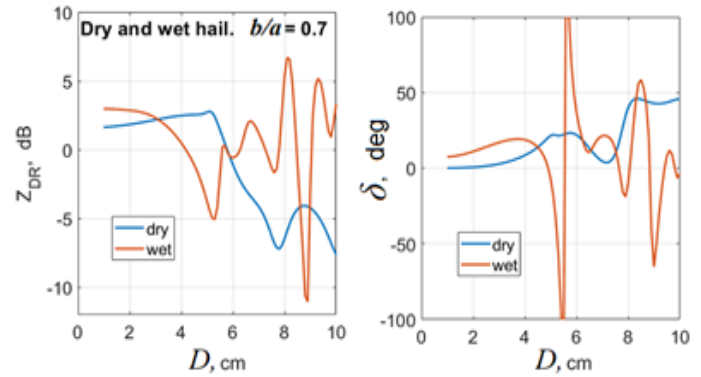


Fig. 4.  $Z_{DR}$  and  $\delta$  as functions of the dimension of horizontally oriented dry and wet hailstones with  $b/a = 0.7$ .

The  $\delta$  values of wet hailstones are significantly larger than those of dry particles at  $D$  less than about 4 cm (Fig. 4, right panel). The same feature can be observed for  $b/a = 0.6$  and  $0.8$  (right panels in Figs. S9 and S10). Large  $\delta$  ( $> 10^\circ$ ) are more probable from wet hail than from dry hail [8, 23]. Our results are in accord with this observation. At moderate  $\langle \theta \rangle$ , hailstones of  $D < 5$  cm can exhibit  $\delta > 10^\circ$  (left central panels in Figs. 5 and S14). Larger hailstones can produce lower and even negative  $\delta$  due to resonances. Notably,  $\delta$  does not significantly depend on  $\beta$ . At intense tumbling,  $\delta$  generally decreases and exhibits more complicated dependencies on  $D$ .

For wet hail with  $D > 4$  cm, the authors of [23] indicate  $\delta > 15^\circ$ . Our results show that smaller  $\delta$  can be produced by larger hailstones having resonance sizes (the curves for  $D = 5$  cm in Figs. 5, S11, S12, S14, and S15). Negative  $\delta$  (Figs. 5, S11, S12, S14, and S15) are produced by hailstones with  $D \approx 5$  cm, which could be used to indicate significantly severe hail. We repeat

> REPLACE THIS LINE WITH YOUR MANUSCRIPT ID NUMBER (DOUBLE-CLICK HERE TO EDIT) <

that in [23], the polarimetric variables are not obtained in the SHV mode and that our main goal is to indicate the effects of  $\beta$  in that mode.

The  $\rho_{hv}$  from wet hailstones exhibits a strong dependence on  $\beta$ . For instance, for  $D = 2$  cm,  $\rho_{hv}$  drops from 0.997 at  $\beta = 0^\circ$  to 0.982 at  $\beta = 90^\circ$  (Fig. 5, left column), which is a significant change. For  $D = 5$  cm, this drop is from 0.995 to 0.974. For resonance sizes,  $\rho_{hv}$  can drop below 0.9 that could be used to detect large hail (Figs. 5 (right column), 6, S14, and S15). At increasing  $\langle\theta\rangle$ ,  $\rho_{hv}$  generally decreases and its dependence on  $\beta$  becomes stronger.

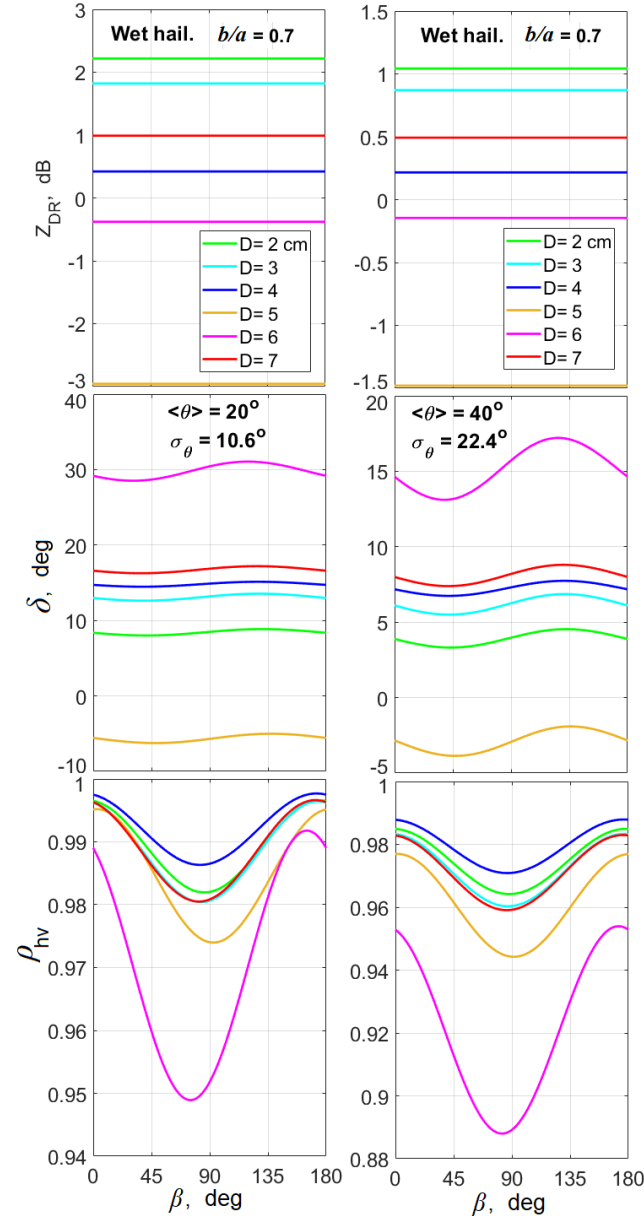


Fig. 5. Wet hailstones. (Left column):  $Z_{DR}$ ,  $\delta$ , and  $\rho_{hv}$  as functions of  $\beta$  for  $\langle\theta\rangle = 20^\circ$ ,  $b/a = 0.7$  and the sizes indicated in the insert. S band. (Right column): As in the left column but for  $\langle\theta\rangle = 40^\circ$ .

Resonance scattering is typically related to sharp changes in the reflected powers or  $Z_{DR}$  as functions of size. For instance,

this effect for wet hailstones can be observed in Fig. 4 at the sizes of about 5, 8.2, and 9 cm. In the right panel of Fig. 4, one can see sharp alterations in the phases at 5.4 (a negative drop) and 5.7 cm (a positive bump). This can be called a resonance effect in the  $\delta$  values that do not correspond to the  $Z_{DR}$  resonance sizes. Fig. 7 and 8 depict  $Z_{DR}$ ,  $\Phi_{DP}$ , and  $\rho_{hv}$  for sizes of 5.4 and 5.7 cm that replace  $D$  of 5 and 6 cm. The  $\delta$  values at  $D = 5.4$  and 5.7 cm (Fig. 7) retain their signs and large values, but strongly depend on  $\beta$ . At random tumbling (Fig. 8), the  $\delta$  and  $\rho_{hv}$  curves for these sizes practically coincide. Because these  $\delta$  resonances occur at close sizes, resulting  $\Phi_{DP}$  can be obtained as the sum of phases from hailstones of  $D = 5.4$  and 5.7 cm that results at much smaller values which could not show the resonances. The  $\rho_{hv}$  values drop strongly (Figs. 7 and 8) and will not change much with this averaging and remain very low. These effects can also be observed in Figs. S26-S28 for  $b/a = 0.6$ . This means that  $\delta$ -resonances in narrow size intervals could not be observed in the  $\Phi_{DP}$ , but very low  $\rho_{hv}$  values can indicate the resonances. The latter feature could be used to indicate wet 5 – 6 cm hail.

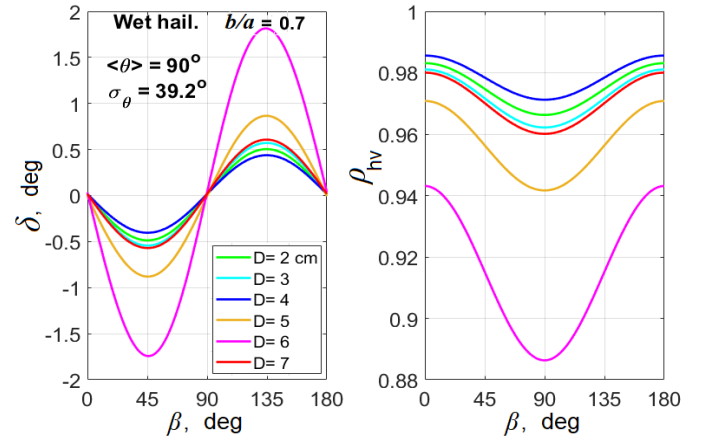


Fig. 6. As in Fig. 5, but for random tumbling.

Our study also shows that the thickness of water cover strongly affects the radar variables. The amount of water on hailstones before water shedding can be larger than that obtained in [26]. It is also known that hailstones can be covered with water in the shape of a toroid [26, 27]. Increasing water content on hailstones shifts the resonance dependencies to smaller sizes; see, for instance, Fig. S17 for spongy hail with volume water content of 0.1. The dielectric constant for spongy hailstones has been calculated using the Maxwell-Garnet equation (e.g., [21] section 1.6) at a temperature of  $0^\circ\text{C}$ . Water or ice have been taken for the matrix. Quite different radar variables have been obtained for the water matrix (Figs. S18-S20) and ice matrix (Figs. S21-S23) with complicated dependencies on  $\langle\theta\rangle$  and  $\beta$ . More research is needed to study these dependencies on water content and composition of ice/water inclusions in water/ice matrices. The WIPL-D allows obtaining the scattering properties of particles having complex compositions. Such a study could verify the Maxwell-Garnet equation for hailstones in wide intervals of ice/water contents and size/shape inclusions.

> REPLACE THIS LINE WITH YOUR MANUSCRIPT ID NUMBER (DOUBLE-CLICK HERE TO EDIT) <

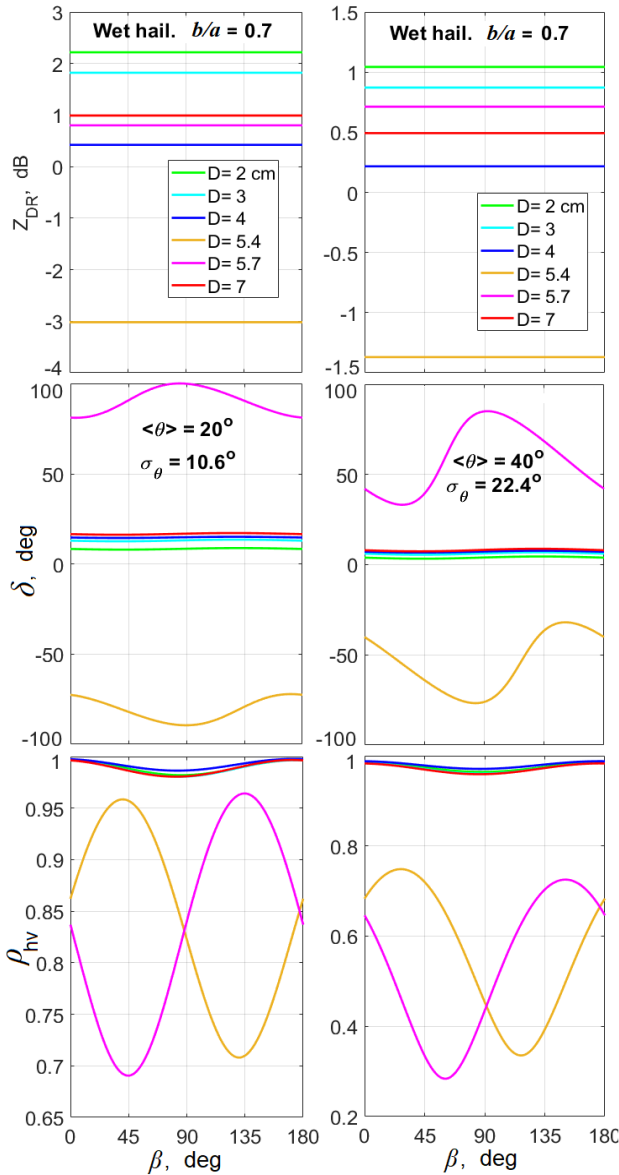


Fig. 7. As in Fig. 5, but for  $D = 5.4$  and  $5.7$  cm instead of  $D = 5$  and  $6$  cm.

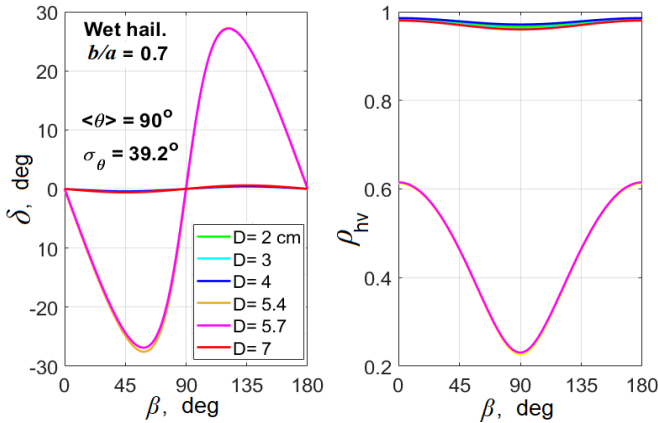


Fig. 8. As in Fig. 6, but for  $D = 5.4$  and  $5.7$  cm (the curves practically coincide) instead of  $D = 5$  and  $6$  cm.

The phase  $\beta$  in precipitation changes with range because the propagation part  $\varphi_{dp}$  increases. The second contribution to  $\beta$  is the phase upon transmission  $\psi_t$  (2). The latter phase is not known on WSR-88Ds and can vary across the network. These variations may lead to different  $\rho_{hv}$  measured with adjacent radars and may produce different results in hail detection. To eliminate the uncertainty caused by  $\beta$ , the phase upon transmission  $\psi_t$  should be measured. If  $\psi_t$  is known,  $\psi_r$  can be readily obtained from  $\Phi_{DP}$  measured in rain areas closest to radar. In these areas,  $\Phi_{DP} = \psi_t + \psi_r$  according to (2) because  $\varphi_{dp}$  and  $\delta$  are negligible and if  $\psi_t$  is known,  $\psi_r$  is obtained from measured  $\Phi_{DP}$ . Then the incident differential phase at any distance in precipitation can be obtained from (2)

$$\beta = (\Phi_{DP} - \psi_r + \psi_t)/2. \quad (18)$$

#### IV. A HAILSTORM

A hail thunderstorm was observed with the WSR-88D KOUN (Norman, OK) on 26 April 2017. The radar can scan in elevation and thus collect vertical cross sections (Fig. 9) called RHIs (Range-Height-Indicators). One can see an enhanced area of  $\Phi_{DP}$  at heights from 4 to 7 km located in the reflectivity core (Fig. 9, bottom panel). The measured differential phase  $\Phi_{DP}$  consists of three contributions: the propagation phase  $2\varphi_{dp}$ , system differential phase  $\psi_t + \psi_r$ , and phase upon scattering  $\delta$  (2). The propagation phase in precipitation increases with range whereas  $\delta$  increases in areas of large scatterers (hailstones) and is small for smaller scatterers (raindrops) at S band.

For a radial at an antenna elevation of  $3.3^\circ$ ,  $\Phi_{DP} = 13^\circ$  at the closest thunderstorm's edge at the distance of 65 km (Fig. 10). This phase is the system differential phase  $\psi_t + \psi_r$ . To analyze the  $\Phi_{DP}$  values along this radial, its range variations are depicted along with  $Z$ ,  $Z_{DR}$ , and  $\rho_{hv}$  (Fig. 10). The  $\Phi_{DP}$  sharply increases at a distance of 67 km ( $\Phi_{DP} = 13^\circ$ ), attains its maximum at a range of 71.75 km ( $\Phi_{DP} = 34^\circ$ ), then decreases and attains a relative minimum at a range of 75 km ( $\Phi_{DP} = 19^\circ$ ). The propagation phase  $2\varphi_{dp}$  increases in range assuming the hydrometeors are nonspherical and have their major axis more aligned with the horizontally polarized wave. The total value of  $2\varphi_{dp}$  is obtained as a difference in  $\Phi_{DP}$  at ranges of 75 and 67 km, i.e.,  $\Delta\Phi_{DP} = 6^\circ$ . The linear increase of the propagation phase is shown in Fig. 10 with the yellow line. The  $\delta$  value at a given distance is obtained as the deviation of  $\Phi_{DP}$  from the yellow line. The maximal deviation is  $19.5^\circ$  at the range of 71.75 km, which is the maximal  $\delta$  for this radial. At that range,  $Z = 62$  dBZ,  $Z_{DR} = 4.6$  dB, and  $\rho_{hv} = 0.986$ . These values of  $Z_{DR}$  and  $\rho_{hv}$  are typically observed in heavy rain, but the  $\delta$  values undoubtedly point to hail presence because of the  $\Phi_{DP}$  hump above the yellow line.

> REPLACE THIS LINE WITH YOUR MANUSCRIPT ID NUMBER (DOUBLE-CLICK HERE TO EDIT) <

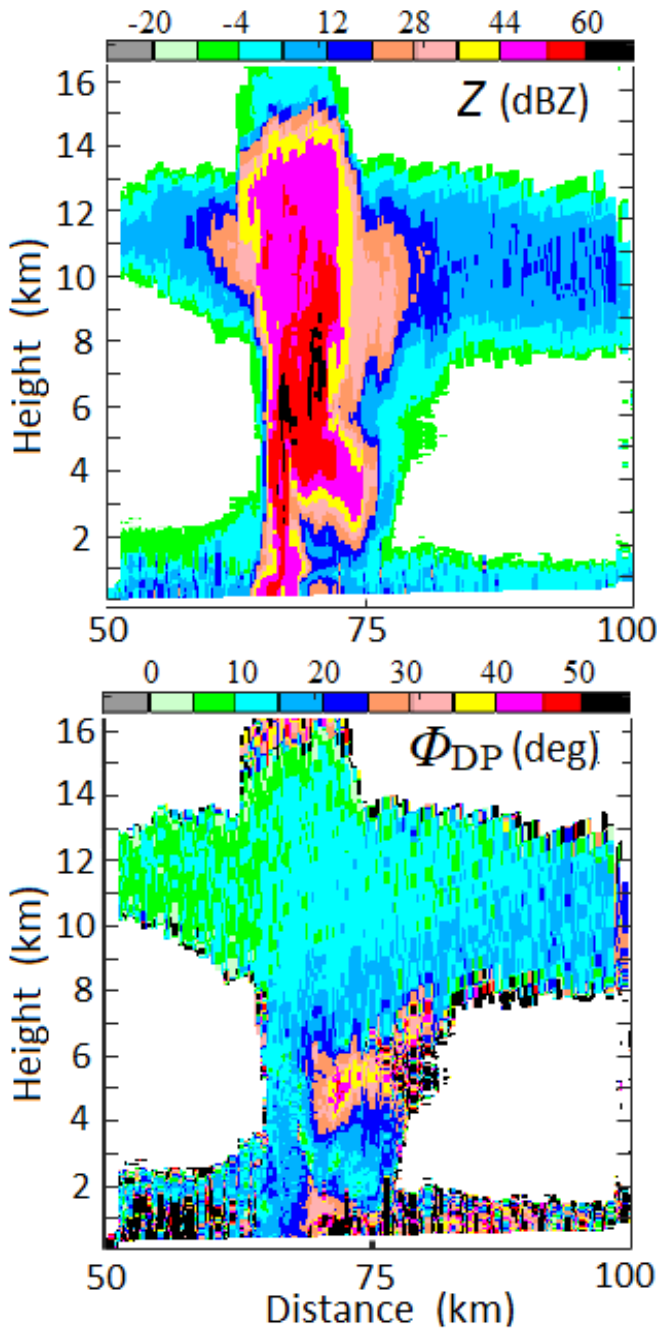


Fig. 9. RHIs of (top) reflectivity and (bottom)  $\Phi_{DP}$  collected with KOUN 26 Apr 2017 at 0300 UTC in an azimuth of 122°.

In the WSR-88D's hail detection procedure, a sliding averaging over 9 successive range gates is utilized [11]. Using such averaging for data in Fig. 10, the following radar variables have been obtained at the range of 71.75 km indicated in Fig. 10 with the dashed line:  $Z = 56$  dBZ,  $Z_{DR} = 3.7$  dB,  $\delta = 10.3^\circ$ , and  $\rho_{hv} = 0.973$ . Figs. S14 and S15 indicate that these  $\delta$  and  $\rho_{hv}$  values can be produced by wet oblate spheroidal hail with  $b/a = 0.6$  and sizes 2-3 cm, but the corresponding  $Z_{DR}$  values are lower than the measured 3.7 dB. There is also a large range of different parameters (hail size, liquid coating thickness and/or distribution within the hailstone, aspect ratio,  $\langle\theta\rangle$ , and a

mixture of hailstones and large raindrops in the radar resolution volume) that can also produce these radar values. The  $Z_{DR}$  and  $\rho_{hv}$  values do not allow detection of hail, whereas measured  $\delta$  undoubtedly indicates hail. The storm did not produce hail at this time [29], 3.8 cm hail was reported at 0346 UTC. Hail indicated with KOUN using  $\delta$  at 0300 UTC could be from the growth stage. The WSR-88D's current hail detection algorithm analyzes reflectivity values at various heights along with thermodynamic parameters. The observed  $\delta$  values unequivocally indicate hail. This points to an advantage of using  $\delta$  in hail detection and sizing.

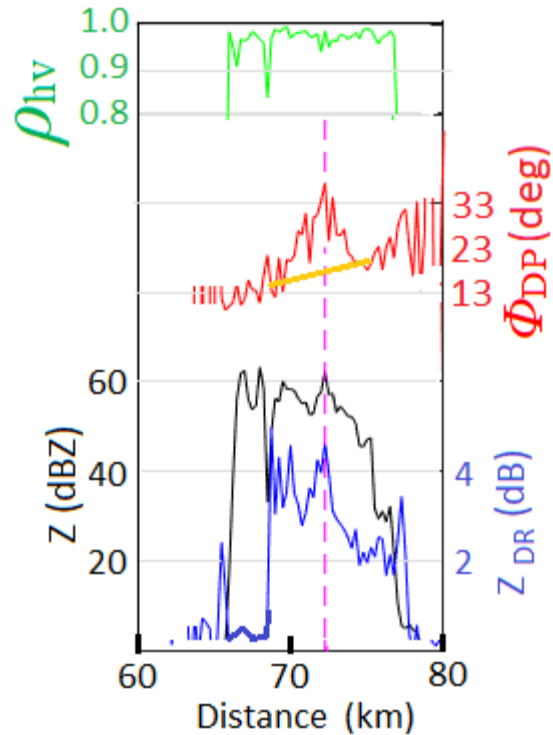


Fig. 10. Range profiles of reflectivity (the black line), differential phase (in red),  $Z_{DR}$  (in blue), and  $\rho_{hv}$  (in green) for an antenna elevation of 3.3° and distances 60 - 80 km. The dashed vertical line is the range marker to read the values of radar variables.

## V. CONCLUSIONS

Radar detection of hail remains challenging. Returned radar signals from hail depend on the hailstones' sizes, shapes, water on and inside hailstones, and tumbling intensity. The polarimetric variables provide more information about scatterers, but the radar detection and sizing of hail remain ambiguous. We show in this paper that the differential phase  $\beta$  of impinging waves in the SHV mode also affects polarimetric variables. On radars employing simultaneous transmission of polarized waves,  $\beta$  contains two parts: the propagation phase acquired in precipitation and the differential phase upon transmission, a radar hardware characteristic, which is typically not known. Therefore, to use polarimetric variables for hail detection and sizing more efficiently, the phase  $\beta$  should be considered.



> REPLACE THIS LINE WITH YOUR MANUSCRIPT ID NUMBER (DOUBLE-CLICK HERE TO EDIT) <

To assess the impacts of  $\beta$ -effect on the radar variables, we have studied oblate spheroidal hailstones. The  $\beta$ -effect is caused by interference of the polarized waves scattered by non-spherical particles. The intensity of interference depends on the orientations of hailstones. We considered scattering using the Euler orientation angles and their Fisher distribution for the probability of orientations. We introduced the mean canting angle  $\langle\theta\rangle$  as a measure of the tumbling intensity of hailstones. At weak tumbling,  $\langle\theta\rangle$  is small and it increases with tumbling intensity. At completely random tumbling,  $\langle\theta\rangle = 90^\circ$ , i.e., an intuitively clear value. Little is known about hailstones' properties in their fall, and we present the results for moderate ( $\langle\theta\rangle = 20^\circ$ ), strong ( $\langle\theta\rangle = 40^\circ$ ), and random ( $\langle\theta\rangle = 90^\circ$ ) tumbling.

If the canting angles are distributed randomly around the vertical (a not too restrictive assumption), then  $Z$  and  $Z_{DR}$  do not depend on  $\beta$  but depend on the tumbling intensity. The phase upon scattering  $\delta$  and correlation coefficient  $\rho_{hv}$  are affected by  $\beta$  and  $\langle\theta\rangle$ ; the  $\beta$ -effect increases with increasing  $\langle\theta\rangle$ .

For dry hail,  $\delta$  increases with increasing hail sizes up to a size of 5 cm at moderate and strong tumbling (Figs. 2, S2, S3, S5, S6). Larger hail exhibits strong resonance impacts, and the latter dependence does not exist. Large hail can be indicated by negative  $Z_{DR}$  and negative  $\delta$ . For wet hail,  $\delta$  increases with hail sizes up to a size of 4 cm beyond which the resonances destroy this dependence. Generally, for hail up to 4 cm,  $\delta$  is larger in wet hail than in dry hail. The  $\beta$ -impact on  $\delta$  is weaker than that on  $\rho_{hv}$ . This makes  $\delta$  a useful variable in hail detection. It is demonstrated in section IV that  $\rho_{hv}$  and  $Z_{DR}$  can have values characteristic of rain, but  $\delta$  values unequivocally indicate hail.

The  $\rho_{hv}$  values from hail depend on hail properties and  $\beta$ . Generally,  $\rho_{hv}$  decreases with decreasing axis ratios and increasing tumbling. Typically,  $\rho_{hv}$  from wet hail is lower than that from dry hail. The  $\beta$ -impact makes utilization of  $\rho_{hv}$  less certain. The  $\rho_{hv}$  is employed in hail detection with WSR-88Ds. Unknown  $\beta$  leads to an uncertainty of utilizing measured  $\rho_{hv}$  quantitatively. To use it more efficiently, the differential phase upon transmission (DPT =  $\psi_t$ ) should be measured because it contributes to  $\beta$ . A method of obtaining DPT on radars capable of vertical sensing is proposed in [30]. However, WSR-88Ds are not capable of fully vertical sensing – their maximal antenna elevation angle is  $60^\circ$ . Therefore, other methods need to be developed to ascertain DPTs for WSR-88Ds.

We present our results for ice spheroids, which approximate natural shapes. Natural hailstones can have shapes with large protuberances/lobes affecting their radar properties [14-16]. A WIPL model of an observed natural hailstone (Fig. S24) has been used to compare its radar properties against ones for a spheroid approximation. The results show (Fig. S25) that the protuberances alter the radar variables of the scatterer that is in accord with [14-16]. To further quantify these impacts, various natural shapes of hailstones should be analyzed at various  $\langle\theta\rangle$  and water covers. WIPL is well suited for such a study.

The hailstorm case in section IV shows that  $Z_{DR}$  can exceed 3 dB, which is a large value typically observed in heavy rain, whereas the  $\delta$  values indicate hail. Such  $Z_{DR}$  can be produced by very oblate hailstones with oblateness of 0.5, but also by less oblate hail having a toroidal water cover. To our knowledge,

scattering properties of the latter type of hailstones have not been studied.

Comparing the results on the  $\beta$ -effect from cloud ice particles above the melting layers [16] and from hail, we highlight two features. a) Oblateness of ice cloud particles can be much stronger than that for small hail and, therefore, the  $\beta$ -impact is stronger on ice cloud particles. b) At S band, the cloud particles are Rayleigh scatterers, whereas hailstones with  $D > 3$  cm can experience resonance scattering and the  $\beta$ -impacts can be strong especially for wet hail.

General conclusions from the presented results at S band are as follows.

- In the SHV polarimetric mode, the differential phase  $\beta$  of impinging waves affects  $\rho_{hv}$  and  $\delta$ ; the impact on  $\rho_{hv}$  is stronger than on  $\delta$ .  $\beta$  does not affect  $Z$  and  $Z_{DR}$  if the canting angles of scatterers are distributed uniformly relative to the vertical.
- The  $\delta$  values do not strongly depend on  $\beta$ , therefore, they can be used quantitatively. The  $\delta$  values from wet hail typically are larger than those from dry hail for sizes up to 5 cm. The  $\delta$  increases with the hail size up to a size of 4 cm that can be used for hail sizing. This dependence breaks for larger hail because of the resonance effects.
- For dry (wet) hail,  $\rho_{hv}$  decreases with its size up to a size of 5 (4) cm. The  $\beta$ -impact on  $\rho_{hv}$  is strong. To use  $\rho_{hv}$  quantitatively for hail sizing, the phase upon transmission of polarized waves should be known (measured).
- Wet hailstones can exhibit very low  $\rho_{hv}$  values ( $< 0.7$ ) from wet hailstones with sizes of 5 - 6 cm having close  $\delta$ -resonances of opposite signs ( $\delta$  panels in Figs. 7 and 8) that could be used to indicate significantly severe hail.
- The incident phase  $\beta$  depends on the differential phase upon transmission and propagation phase through precipitation. For adjacent radars sensing the same area, both phases may differ. Values of  $\rho_{hv}$  depend on  $\beta$ . Therefore,  $\rho_{hv}$  values measured from adjacent radar from the same hail area can differ and impact hail detection based on  $\rho_{hv}$ .
- $Z_{DR}$  and  $\rho_{hv}$  values from thunderstorms can have rain values, whereas  $\delta$  can unequivocally indicate hail presence.

To estimate the hail size, several hailstones' properties affecting radar returns should be analyzed: their shapes, wetness, the intensity of tumbling, and the  $\beta$ -effect. This multiparameter dependence makes hail sizing challenging. The  $\delta$  values can bring additional information to the hail detection method based on  $Z$ ,  $Z_{DR}$ , and  $\rho_{hv}$  currently employed on WSR-88Ds. More information about scatterers could be obtained with radars capable of changing their differential phase upon transmission. Measured  $\delta$  and  $\rho_{hv}$  at various DPTs could be used as additional variables for the retrievals. DPT can be changed with a high-power phase shifter (e.g., [31]) that complicates radar hardware. On modern radars with digital transmitters and on phased array radars, more control is available on transmit



> REPLACE THIS LINE WITH YOUR MANUSCRIPT ID NUMBER (DOUBLE-CLICK HERE TO EDIT) <

pulses and DPT can be altered by delaying the transmitted polarized waves relative to each other.

#### ACKNOWLEDGMENT

We thank Edwin Dunnavan, Matthew Kumjian, and the reviewers for their comments which helped us to improve the manuscript.

#### REFERENCES

- [1] A. Witt, M. D. Eilts, G. J. Stumpf, J. T. Johnson, E. D. Mitchell, and K. W. Thomas, "An enhanced hail detection algorithm for the WSR-88D", *Wea. Forecasting*, vol. 13, pp. 286-303, 1998.
- [2] A. Witt, M. D. Eilts, G. J. Stumpf, E. D. Mitchell, J. T. Johnson, and K. W. Thomas, "Evaluating the performance of WSR-88D severe storm detection algorithms", *Wea. Forecasting*, vol. 13, pp. 513-518, 1998.
- [3] S. Blair, D.R. Deroche, J.M. Boustead et. al: "A radar-based assessment of the detectability of giant hail". *Elec. J. Severe Storms Meteor.*, 6, 1-30, 2011 <https://ejssm.org/archives/wpcontent/uploads/2021/09/vol6-7.pdf>
- [4] V. N. Bringi, T. A. Seliga and K. Aydin, "Hail detection with differential reflectivity radar", *Science*, vol. 225, pp. 1145-1147, 1984.
- [5] K. Aydin, T. Seliga and V. Balaji, "Remote sensing of hail with a dual linear polarization radar," *J. Climate Appl. Meteorol.*, vol. 25, no. 10, pp. 1475-1484, 1986.
- [6] T. A. Seliga and V. N. Bringi, "Differential reflectivity and differential phase shift: Applications in radar meteorology," *Radio Science*, vol. 13, no. 2, pp. 271-275, 1978.
- [7] K. Aydin and Y. Zhao, "A computational study of polarimetric radar observables in hail," *IEEE Trans. Geosci. Remote Sens.*, vol. 28, pp. 412-422, 1990.
- [8] N. Balakrishnan and D. S. Zrnic, "Use of polarization to characterize precipitation and discriminate large hail," *J. Atmos. Sci.*, vol. 47, pp. 1525-1540, 1990.
- [9] A. V. Ryzhkov, M. R. Kumjian, S. M. Ganson and P. Zhang, "Polarimetric radar characteristics of melting hail. Part II: Practical implications," *J. Appl. Meteorol. Climatol.*, vol. 52, pp. 2871-2886, 2013.
- [10] K. L. Ortega, J. M. Kraus and A. V. Ryzhkov, "Polarimetric Radar Characteristics of Melting Hail. Part III," *J. Appl. Meteor. Climatol.*, vol. 55, pp. 829-848, 2016.
- [11] H. S. Park, A. V. Ryzhkov, D. S. Zrnic and K. E. Kim, "The hydrometeor classification for polarimetric WSR-88D; description and application to an MCS," *Wea. Forecasting*, vol. 24, pp. 730-748, 2009.
- [12] B. M. Kolundzija, "Electromagnetic modeling of composite metallic and dielectric structures," *IEEE Trans. Microwave Theory and Techniques*, vol. 47, no. 7, pp. 1021-1032, 1999.
- [13] E. Chobanyan, N. Sekeljic, M. M. Ilic, V. N. Bringi and B. Notaros, "Efficient and accurate computational electromagnetics approach to precipitation particle scattering analysis based on higher-order method of moments integral equation modeling," *J. Atmos. Oceanic Technol.*, vol. 32, pp. 11745-11758, 2015.
- [14] Z. Jiang, M. R. Kumjian, R. R. Schrom, I. Giammanco, T. Brown-Giammanco, H. Estes, R. Maiden and A. J. Heymsfield, "Comparisons of electromagnetic scattering properties of real hailstones and spheroids". *J. Appl. Meteorol. Climat.*, **58**, 93-112, 2019.
- [15] M.A. Cecchini, A. Heimsfield, R. Honeyager, et. al: "Revisiting the hail radar reflectivity-kinetic energy flux relation by combining T-matrix and discrete dipole approximation calculations to size distribution observations", *J. Atmos. Sci.*, 79, pp.1927-1940, 2022.
- [16] M.R. Kumjian, J. Schrom, Soderholm, and I. Giammanco: "Radar and hail: advances in scattering, detection, and sizing. Chapter 4 in *Advances in Weather Radar Volume II*, V. Bringi, ed., IET Press, pp. 143-207, 2024.
- [17] D. Mirković, D. S. Zrnić, V. Melnikov, and P. Zhang, "Effects of rough hail scattering on polarimetric variables". *IEEE Trans. GRS*, 2021.
- [18] D. Zrnić, R. Doviak, G. Zhang, and A. Ryzhkov, "Bias in differential reflectivity due to cross coupling through the radiation pattern of polarimetric weather radars," *J. Atmos. Oceanic Technol.*, vol 27, N. 10, pp. 1624-1637, 2010.
- [19] V. Melnikov, "Impacts of the phase shift between incident radar waves on the polarization variables from ice cloud particles". *J. Atmos. Oceanic Technol.*, vol 37, pp. 1423-1436, 2020.
- [20] K.V. Mardia, "Statistics of Directional Data", NY, Academic Press, 1972. 357 pp.
- [21] V.N. Bringi and V. Chandrasekar, *Polarimetric Doppler Weather Radar. Principles and Applications*". Cambridge University Press, 2001, 636 pp.
- [22] WIPL d.o.o, "WIPL-D Electromagnetic Simulation Software," 2021. Available online: [www.wipl-d.com](http://www.wipl-d.com). [Accessed 11/10/2021].
- [23] J.M. Straka, D. S. Zrnic, and A. V. Ryzhkov, "Bulk hydrometeor classification and quantification using polarimetric radar data: Synthesis of relations. *J. Appl. Meteor.*, v. 39, pp. 1341-1372, 2000.
- [24] L. Shedd, M. Kumjian, I. Giammanco, T. Brown-Giammanco, and B.R. Maiden, "Hailstone shapes", *J. Atmos. Sci.*, v. 78, pp. 639-652, 2021.
- [25] M. R. Kumjian, R. Gutierrez, J. S. Soderholm, et al.: "Gargantuan hail in Argentina", *Bull. Amer. Meteorol. Soc.*, 101(8), pp. E1242 - E1258, 2020. <https://doi.org/10.1175/BAMS-D-19-0012.1>
- [26] R.M. Rasmussen and A. J. Heymsfield, "Melting and shedding of graupel and hail. Part I: Model physics", *J. Atmos. Sci.*, vol. 44, pp. 2754-2763, 1987.
- [27] H.R. Pruppacher and J. D. Klett "Microphysics of Clouds and Precipitation." Kluwer Academic, 954 pp., 1997.
- [28] V.N. Bringi, R. M. Rasmussen, and J. Vivekanandan, "Multiparameter radar measurements in Colorado convective storms. Part I: Graupel melting studies. *J. Atmos. Sci.*, 43, 2545-2563, 1986
- [29] Hail reports data source: [https://www.spc.noaa.gov/climo/gmf.php?rpt=170425\\_rpts\\_filtered](https://www.spc.noaa.gov/climo/gmf.php?rpt=170425_rpts_filtered)
- [30] D.S. Zrnić and V. Melnikov, "Estimation of transmitted differential phase on dual polarization radars", *J. Atmos. Oceanic Technol.*, 40 (10), pp. 1221-1239, 2023.
- [31] A.C. Schroth, M.S. Chandra, and P. Meischner: "C-band coherent polarimetric radar for propagation and cloud physics research". *J. Atmos. Oceanic Technol.*, vol 5, n. 12, pp. 803-822, 1988.